

# Supernova Relic Neutrinos in Liquid Argon detectors

A . G . Cocco, A . Ereditato, G . Fiorillo, G . Mangano  
and V . Pettorino

Dipartimento di Scienze Fisiche, Università di Napoli "Federico II",  
and INFN, Sezione di Napoli,  
Complesso Universitario di Monte Sant'Angelo, Via Cintia, I-80126 Napoli, Italy

**Abstract.** We study the possibility of detecting the background of Supernova Relic Neutrinos (SRN) with liquid Argon Time Projection Chamber (TPC) detectors. As far as this study is concerned, these experimental devices are mainly sensitive to electron neutrino signals, and could provide further information on both Supernova explosion mechanism and on star formation rate at redshifts  $z \sim 2$ . We study in details the main contributions to background in the relevant energy range from  ${}^8\text{B}$  and hep solar neutrinos as well as from low energy atmospheric neutrino fluxes. Depending on the theoretical prediction for the SRN flux we find that for a 3 kton and a 100 kton liquid Argon TPC detectors the signal may be observed at the 1 and 4 level, respectively, with 5 years of data taking.

PACS numbers: 13.15.+g, 97.60.Bw, 14.60.Pq

x alfredo.cocco@na.infn.it  
antonio.ereditato@na.infn.it  
giuliana.orillo@na.infn.it  
gianpiero.mangano@na.infn.it  
valeria.pettorino@na.infn.it

## 1. Introduction

Type II Supernova explosions (SN II) are among the most energetic events in the Universe known so far. Massive stars with mass larger than about eight solar masses undergo several burning phases until the compact core has been fused into iron. Lacking any further source of nuclear energy to balance gravity, the star collapses. When the inner core reaches nuclear densities an outward propagating shock wave is produced, which eventually leads to a huge luminosity release of the order of  $10^{53}$  erg and to the explosion of the outer layers of the star. This huge energy flux is almost entirely in the form of neutrinos of all flavors produced via weak processes which diffuse through the very dense inner part of the structure and eventually freely escape from the neutrinosphere, cooling the remnant proto-neutron star on a time scale of 10 seconds.

This SN II model has been confirmed by the detection of neutrinos from the SN 1987A [1], [2], though the small number of observed events still leaves important issues unsolved, as for example the shock revival mechanism, the way the flux is distributed among the neutrino and antineutrino flavors, and finally a detailed knowledge of the neutrino mean energies at the neutrinosphere. For a recent review on this and related issues see e.g. [3].

Future nearby SN II events would probably provide enough information to achieve a deeper understanding of the core-collapse mechanism, since many running experiments, such as Super-Kamiokande [4], SNO [5], KamLAND [6] and LVD [7], as well as others under construction, like ICARUS [8],[9], will collect a huge number of neutrino events, of the order of  $10^4$ . Waiting for such an event, whose rate is typically estimated to be of a few per century in our galaxy, it is interesting to study the possibility to detect with present and future experiments the isotropic neutrino flux due to all SN II that have occurred so far in the Universe. This would represent an independent probe of SN II mechanism, as well as of the SN II rate as a function of redshifts up to  $z \approx 3$ . The latter, being simply proportional to the star formation rate for stars heavier than  $8M_{\odot}$ , is an important cosmological observable that is presently studied via optical and UV surveys but that is still poorly known at high redshifts.

The expected Supernova Relic Neutrino (SRN) flux has been considered by several authors [10]–[14], and the results span quite a wide range, mainly because of different modelling of the star formation rate versus  $z$ . All these predictions but the one of the simplest constant supernova rate model [10] are compatible with the present experimental upper bound on  $\Phi_{\nu_e}$  flux obtained by the Super-Kamiokande Collaboration,  $(\Phi_{\nu_e}) < 1.2 \text{ cm}^{-2} \text{ s}^{-1}$  for neutrino energies higher than 19.3 MeV [15]. A forecast for future possible detection of the signal in this experiment, as well as in KamLAND, has been considered in [16]. The authors find that, by adopting a model which is still compatible with the Super-Kamiokande bound and which is also motivated by UV density studies and by the Sloan Digital Sky Survey cosmic optical spectrum bounds on the  $z$  behavior of the star formation rate [17],[18], the SRN background may be detected at the 1  $\sigma$  level in a few years of running.

In this paper we consider the possibility of measuring the SRN signal by using a different class of experiments based on the liquid Argon TPC (Time Projection Chamber) technique [19]. Presently, this experimental method is adopted in the ICARUS experiment whose final 3 kton configuration (T3000) is planned to be commissioned at the INFN Gran Sasso Underground Laboratories in the near future [8]. We note that large mass liquid Argon TPC detectors (100 ktons) have been also considered as powerful experimental devices for next generation neutrino physics and in particular as SN II neutrino flux detectors [20].

Though with different efficiencies, experiments like ICARUS are sensitive to all neutrino flavors. As we will discuss in Section 3, neutrinos and antineutrinos interact via neutral current with Argon nuclei, as well as by elastic scattering off electrons. Finally, electron neutrinos can also undergo charged current interactions, which indeed are the leading processes with the highest cross section. Electron antineutrino charged current interactions are typically at least one order of magnitude smaller. It is worth stressing that the SRN signal would be mainly detected in this case in its  $\bar{\nu}_e$  component, so that ICARUS-like experiments provide a complementary piece of information with respect to Super-Kamiokande or KamLAND, which instead constrain the  $\bar{\nu}_e$  flux.

The main background sources for SRN events, in the relevant neutrino energy range of 10–50 MeV, are given by solar and low energy atmospheric neutrinos. These fluxes are indeed large enough to completely overwhelm the SRN signal at low energies, lower than the  $^8\text{B}$  neutrino flux endpoint at approximately 16 MeV, as well as for sufficiently high energies where the atmospheric neutrino flux becomes the dominant contribution. However, in the intermediate energy range of 18–40 MeV the expected SRN signal is likely to represent a substantial fraction of the total flux. By suitably choosing the energy window, fluxes as the one considered in [16] may therefore be detectable.

This paper is organized as follows. In Section 2 we review the main features of SRN fluxes and we introduce the fiducial model used in our analysis. Section 3 covers the neutrino interaction processes in liquid Argon TPCs. The expected energy spectrum and event rate from SRN as a function of the star formation rate and the effect of the resonant neutrino oscillations in the outer Supernova matter layers is studied in Section 4. We also discuss the backgrounds from solar and atmospheric neutrinos and the corresponding electron signals and compare these backgrounds with the SRN flux. Finally, we report our conclusions in Section 5.

## 2. Supernova Relic Neutrino Background

The neutrino differential flux  $\Phi(E)$  (number of neutrinos per energy interval, per unit time and per unit area) from past SN II exploded in our observable Universe can be written as follows

$$\Phi(E) = c \int_0^{z_{\text{max}}} \frac{dz}{H(z)} R_{\text{SN}}(z) hN(E(1+z)) i ; \quad (2.1)$$

where  $\nu$  denotes the neutrino or antineutrino flavor and  $H(z)$  is the Hubble parameter

$$H(z) = H_0 \left[ \Omega_m (1+z)^3 + \Omega_R (1+z)^4 + (1 - \Omega_m - \Omega_R) (1+z)^2 \right]^{1/2} \quad (2.2)$$

Since SN II produce equal fluxes for  $\nu$  and  $\bar{\nu}$  neutrino/antineutrino, in the following we will collectively denote these states as  $\nu_x$  and  $\bar{\nu}_x$ . In Equation (2.2)  $H_0 = 100 \text{ h km s}^{-1} \text{ M pc}^{-1}$  is the present value of the Hubble parameter, with  $h = 0.7 \pm 0.1$  [21], [22], while  $R_{\text{SN}}$  in Equation (2.1) is the SN II rate per unit time and comoving volume and  $\langle N_i \rangle$  is the number of  $\nu_i$  emitted per unit of initial unredshifted energy by a SN II averaged over the stellar initial mass function and evaluated at  $E/(1+z)$ , where  $E$  is the energy measured on earth.

In the following we consider a spatially flat  $\Lambda$ CDM model with  $\Omega_m = 0.3$ ,  $\Omega_R = 0.7$  and  $\Omega_\Lambda = 0$ . The value of  $z_{\text{max}}$  is typically set by the experimental threshold on the lowest detectable neutrino energy. In fact, with increasing  $z$  the energy of neutrinos at production, which is typically of order of  $10 \text{ MeV}$ , is redshifted towards smaller values which eventually become difficult to be measured.

The Supernova rate  $R_{\text{SN}}(z)$  is the star formation rate for stellar masses larger than  $8M_\odot$ . Several models have been considered in the recent literature [10]–[14], whose predictions for the neutrino flux vary by approximately one order of magnitude. For our analysis we will consider a fiducial model as in [16]

$$\begin{aligned} R_{\text{SN}}(z) &= R_0 (1+z)^\alpha; & z < 1 \\ &= R_0 2^\beta (1+z)^\alpha; & z > 1 \end{aligned} \quad (2.3)$$

where the present rate  $R_0$  is estimated in the range  $(0.7 \pm 0.4) \times 10^4 \text{ yr}^{-1} \text{ M pc}^3$  [16], [17]. Limits on the slope parameters have been found in [18] using the Sloan Digital Sky Survey optical spectrum giving the ranges  $2 \pm 3$  and  $0 \pm 2$ . In particular, all our results given in the following are obtained using  $R_0 = 2 \times 10^4 \text{ yr}^{-1} \text{ M pc}^3$ . Corresponding estimates for higher or lower values of  $R_0$  can be obtained straightforwardly, since this parameter linearly enters the neutrino differential flux. We also choose  $\alpha = 2.5$  and  $\beta = 1$ , but we discuss in the following how our findings are affected when these parameters vary in the ranges shown above.

The second important input of Equation (2.1) is the neutrino spectrum emitted by a SN II, which should be averaged over the mass distribution. Actually, all relevant properties which characterize the neutrino spectrum are only weakly depending on the mass of the star, at least for not very heavy stars. We will therefore make the assumption that the mass average can be approximated by the neutrino spectrum of a typical Supernova. This spectrum is obtained by numerically solving the explosion dynamics [3] and can be parameterized with good accuracy by a Fermi-Dirac distribution

$$N(E) = k \frac{L_{\text{SN}}}{T^4} \frac{E^2}{\exp(E/T) + 1}; \quad (2.4)$$

where  $L_{\text{SN}}$  is the Supernova luminosity,  $T$  the effective temperature and  $k$  is usually known as pinching parameter. Finally, the constant  $k$  is chosen so that the first moment of the distribution is normalized to the total energy emitted in the

|     | mass hierarchy  | $\theta_{13}$ | $P(\nu_e \rightarrow \nu_e)$ | $P(\bar{\nu}_e \rightarrow \bar{\nu}_e)$ |
|-----|-----------------|---------------|------------------------------|--|
| I   | normal          | large         | $\sin^2 \theta_{13}$         | $\cos^2 \theta_{12}$                     |
| II  | inverted        | large         | $\sin^2 \theta_{12}$         | $\sin^2 \theta_{13}$                     |
| III | normal/inverted | small         | $\sin^2 \theta_{12}$         | $\cos^2 \theta_{12}$                     |

Table 1. The  $\nu_e$  and  $\bar{\nu}_e$  survival probability due to MSW resonances in a SN II, as function of neutrino mass hierarchy and  $\theta_{13}$  mixing angle.

channel. Typical values for these parameters, which will be adopted in our study, are the following

$$\begin{aligned} T_e &= 3.5 \text{ M eV}; & T_{\bar{e}} &= 5 \text{ M eV}; & T_x &= 8 \text{ M eV}; \\ \theta_e &= 2; & \theta_{\bar{e}} &= 2; & \theta_x &= 1; \end{aligned} \quad (2.5)$$

We consider a total luminosity  $L_{\text{SN}} = 3 \cdot 10^3 \text{ erg}$  that is equally distributed among the neutrino/antineutrino species.

Neutrino fluxes from a SN II as measured on earth are influenced by oscillation phenomena. Once produced at neutrinosphere, neutrinos propagate in the outer star layers and experience two MSW resonances at different densities (see e.g. [23]). The first resonance governed by atmospheric mass splitting and the value of the small mixing angle  $\theta_{13}$  occurs at  $10^3 \text{ g cm}^{-3}$  ( $10 \text{ M eV} = E$ ). At a lower density of  $10^2 \text{ g cm}^{-3}$  ( $10 \text{ M eV} = E$ ) a second resonance takes place determined by the solar parameters  $\theta_{12}^2$  and  $\theta_{12}$ . For the experimentally favored Large Mixing Angle (LMA) solution of the solar neutrino problem this second resonance satisfies the adiabatic condition for all realistic matter profiles in a SN II. On the other hand, depending on the neutrino mass hierarchy and the value of  $\theta_{13}$ , the higher density resonance occurs in the neutrino or in the antineutrino sectors and can be fully adiabatic or rather maximally violating adiabaticity. Correspondingly, the survival probabilities take different values, as shown in Table 1 where we consider the two limiting cases of large and small  $\theta_{13}$  mixing angle,  $\sin^2 \theta_{13} = 10^{-3}$  and  $\sin^2 \theta_{13} = 10^{-6}$ , respectively. For intermediate values of  $\theta_{13}$  the survival probability depends on neutrino/antineutrino energy, but this effect is completely negligible for the SRN neutrino flux detection we are interested in, which is only weakly sensitive to the value of  $\theta_{13}$ .

The effect of oscillations on SRN event will be discussed in the following. We use the LMA solution for solar neutrino problem which gives as best value  $\sin^2 \theta_{12} = 0.3$  [24]. Since  $\nu_x$  are produced with a higher mean energy we expect that in case I, which implies that all detected  $\nu_e$  were born at neutrinosphere as  $\nu_x$ , the number of SRN events would be larger. In fact, the cross section for charged current interaction of  $\nu_e$  with Argon nuclei, which is the leading interaction channel, grows with energy more rapidly than neutrino energy to the first power. The two scenarios II and III give instead very close results.

### 3. Neutrino detection with Liquid Argon TPC detectors

Neutrinos are identified in liquid Argon TPCs via charged and neutral current interactions on Argon nuclei, as well as from elastic scatterings on atomic electrons [8]. In both cases the final state is mainly electromagnetic, allowing for an efficient detection. The excellent properties of liquid Argon as an electromagnetic calorimeter medium allow to work with a low detection threshold and a high resolution energy measurement. In this paper we will refer in particular to the ICARUS detector that combines the features of a bubble chamber as far as the spatial resolution and the particle identification are concerned, to those of an electronic TPC. The detector is continuously active and sensitive, self-triggering and able to perform high-quality imaging even of low energy events such as those due to the interaction of neutrinos from stellar collapses.

We now discuss in details the cross sections for the relevant neutrino interaction processes.

Electron neutrino charged current interactions on Argon



proceed via the creation of an excited state of  ${}^{40}\text{K}$  and its subsequent gamma decay. The threshold for this process is given by the sum of the known  $Q$ -value of the inverse reaction (beta decay of  ${}^{40}\text{K}$ ,  $Q = 1.505 \text{ MeV}$ ) and the energy needed to produce the given excited state of the  ${}^{40}\text{K}$ . At low energy, as discussed in [25], the main contribution to the cross section is from a Fermi transition to the isobaric analog state of  ${}^{40}\text{K}$  and Gamow-Teller transitions to three low-lying  ${}^{40}\text{K}$  states. Details are shown in Table 2.

The charged current interaction cross section at higher neutrino energies ( $30 \text{ MeV} < E < 100 \text{ MeV}$ ) has been evaluated in [26] by using a Random Phase Approximation calculation. Levels up to  $J=6$  have been taken into account. A plot of the cross section is shown in Figure 1.

A similar analysis of the  $\bar{\nu}_e$  charged current process



have been also carried out in [26]. This process has a higher neutrino energy threshold of  $7.48 \text{ MeV}$ . The corresponding cross section is also reported in Figure 1. Notice that charged current cross sections grow with neutrino energy more rapidly than  $E^{-2}$  to the first power.

For relatively low energy transfer from the neutrino, neutral current reactions on Argon nuclei proceed via the excitation of nuclear resonances decaying back to Argon ground state with the emission of one or more photons



A study of nuclear levels of Argon reveals that the most energetic photon emitted in this process has an energy not exceeding  $11 \text{ MeV}$  [27]. These photons typically produce Compton electrons or electron/positron pairs, which however have energies

| Transition   | Excitation level (MeV) | Branching Ratio (%) |
|--------------|------------------------|---------------------|
| Fermi        | 4.384                  | 32.76               |
| Gamow-Teller | 3.798                  | 13.69               |
| Gamow-Teller | 3.11                   | 18.16               |
| Gamow-Teller | 2.73                   | 28.94               |

Table 2. Nuclear excitation levels for  $^{40}\text{K}$  used in the analysis. See [25] for further details.

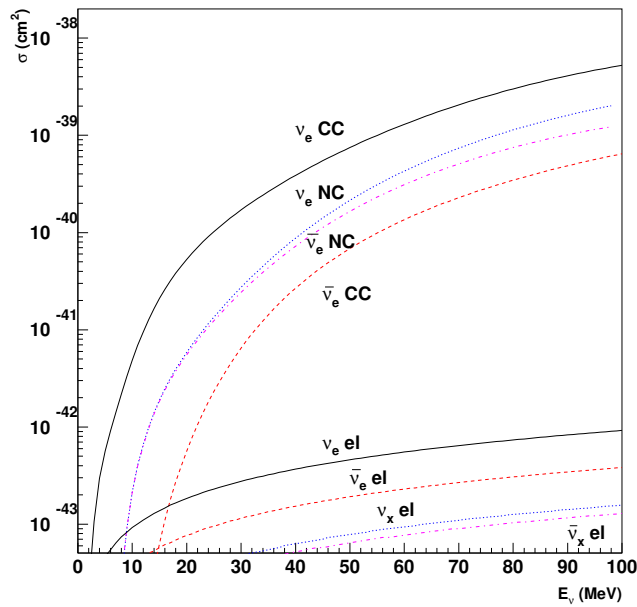


Figure 1. The cross section for neutrino interaction processes in liquid Argon. From top to bottom, charged current  $\nu_e$ Ar, neutral current  $\nu_e$ Ar, neutral current  $\bar{\nu}_e$ Ar, charged current  $\bar{\nu}_e$ Ar, and elastic scattering for  $\nu_e$ ,  $\bar{\nu}_e$ ,  $\nu_x$  and  $\bar{\nu}_x$  on electrons. The neutral current results are from [9].

lying outside the energy range we are interested in. In fact, as we will see in the following, the SRN signal to background ratio is expected to be maximal by selecting the outgoing electron (positron) energy range above the threshold given by the steep rising of  $^8\text{B}$  solar neutrino flux, at approximately 16 MeV. We also note that there is experimental evidence for a giant quadrupole resonance at 17.7 MeV [27], which is likely to produce multiphoton transition to ground state. In this case too de-excitation of Argon would produce electrons with energy smaller than 16 MeV. Finally, for higher excitation energies, Argon nuclei are no longer stable and the final state contains one or more nucleons and a remnant nucleus, which can be distinguished from a single outgoing electron signal in liquid Argon TPC. As a consequence, in the following we will not consider neutral current interactions.

Elastic neutrino electron scattering cross sections, shown in Figure 1, have a linear dependence on neutrino energy  $E$

$$(\bar{\nu}_e e \rightarrow \bar{\nu}_e e) = 9.20 \cdot 10^{45} (E \text{ MeV}) \text{ cm}^2 ; \quad (3.4)$$

$$(\nu_e e \rightarrow \nu_e e) = 3.83 \cdot 10^{45} (E \text{ MeV}) \text{ cm}^2 ; \quad (3.5)$$

$$(\bar{\nu}_e ; e \rightarrow \bar{\nu}_e ; e) = 1.57 \cdot 10^{45} (E \text{ MeV}) \text{ cm}^2 ; \quad (3.6)$$

$$(\nu_e ; e \rightarrow \nu_e ; e) = 1.29 \cdot 10^{45} (E \text{ MeV}) \text{ cm}^2 ; \quad (3.7)$$

Notice that the above cross sections are many orders of magnitude smaller than the one for charged current  $\nu_e$  interactions. As we will see in the following, elastic scattering gives a very small contribution to the total SRN neutrino event rate in liquid Argon detectors.

With the exception of neutral currents, all the processes considered above include one electron (or positron) in the final state and typically one or more photons. We will assume that electrons above 5 MeV can be measured with full efficiency in the detector, despite the presence of de-excitation photons [8]. The latter could be possibly used to improve the knowledge on the incoming neutrino energy.

As we already mentioned, liquid Argon TPC detectors have good capabilities in the reconstruction of electromagnetic showers. As reported by the ICARUS Collaboration, the energy resolution can be parameterized as follows [28]

$$\frac{\sigma(E_e)}{E_e} = \sigma \frac{11\%}{E_e \text{ (MeV)}} + 2.5\% ; \quad (3.8)$$

in the neutrino energy range relevant for this analysis.

#### 4. SRN signal and backgrounds

There are two main sources of background for the SRN signal in the energy range 10–50 MeV. For energies lower than approximately 20 MeV the (largely) dominant contribution comes from  ${}^8\text{B}$  and hep solar neutrinos. These fluxes are quite accurately known. In Figure 2 we show the results of the standard solar model by Bahcall and Pinsonneault [29]. Total fluxes are chosen according to the best values suggested in [29], namely  $\Phi_{\text{B}} = 5.79 (1.0 \pm 23) \cdot 10^6 \text{ cm}^{-2} \text{ s}^{-1}$  and  $\Phi_{\text{hep}} = 7.88 (1.0 \pm 16) \cdot 10^6 \text{ cm}^{-2} \text{ s}^{-1}$ , while the energy profile has been obtained with the data given in [30] (see also [31]). The  ${}^8\text{B}$  flux is dominating the  $\nu_e$  flux up to an energy of 15 MeV, while hep neutrino flux extends well beyond up to 18.8 MeV.

At higher energies the atmospheric neutrino background becomes dominant. The estimated flux for  $\nu_e$  down to an energy of 10 MeV at the underground Gran Sasso Laboratory is shown in Figure 2 [32], as predicted by the FLUKA Monte Carlo package [33]. There is a systematic error in the evaluation of the atmospheric neutrino flux, due to uncertainties both in the absolute flux of primary cosmic rays producing neutrinos and in the cross section for hadronic interactions. We assume in the following a 30% relative uncertainty as a conservative estimate for these systematic effects [32].

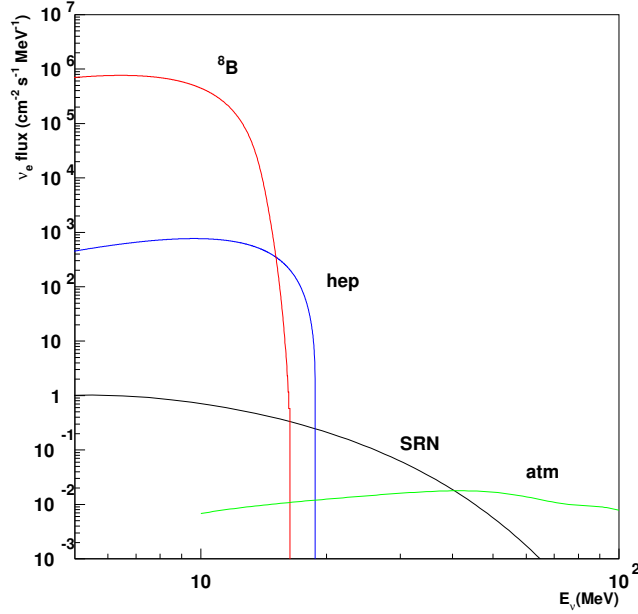


Figure 2. The expected SRN flux of  $\nu_e$  for the model of Section 2, a normal neutrino mass hierarchy and  $\sin^2 \theta_{13} = 0.02$ . The  $^8\text{B}$  and hep solar fluxes are also shown together with the atmospheric  $\nu_e$  flux.

Assuming the reference model considered in Section 2, we find an interesting energy window where the SRN signal can be detected, at least in principle. From Figure 2 we notice that from the hep endpoint at 19 MeV up to energies as high as 40 MeV the SRN  $\nu_e$  give a relevant contribution to the total expected flux. Actually, this prediction strongly depends on the estimated SRN flux. For those models which predict a lower flux this energy window can become much smaller or even disappear. In any case, we see that any attempt to detect the SRN signal, in particular in its  $\nu_e$  component, requires a preliminary analysis of the possible signal to background ratio in the 20–40 MeV energy range.

For this purpose we have simulated about  $10^4$  SRN events according to a SN II spectrum whose parameters are chosen as in Equation (2.5) along with  $10^4$  and  $10^5$  solar and atmospheric neutrino events, respectively. Incoming neutrino spectra have been normalized to the expected fluxes. We consider a normal neutrino mass hierarchy and a large value for the  $\theta_{13}$  mixing angle (case I of Table 1). Interaction of these fluxes with the detector proceeds via charged current or elastic scattering. We use as detection signature the electron (positron) produced in the charged current interaction, or the recoil electron for elastic scattering. The electron (positron) energy  $E_e$  spectra is reconstructed by using the corresponding differential cross section  $d\sigma/dE_e$  which has a well known behavior in standard electroweak theory, and taking into account the thresholds and detection efficiency described in Section 3.

Results are shown in Figure 3, where the number of events due to solar, atmospheric and SRN neutrinos is given as a function of the electron (positron) energy, in the energy window 12–50 MeV. The signature of SRN neutrino induced events for  $16 \leq E_e \leq 40$  MeV is more clearly seen in Figure 4 where we compare the total event energy spectrum with the one expected for the solar and atmospheric backgrounds only.

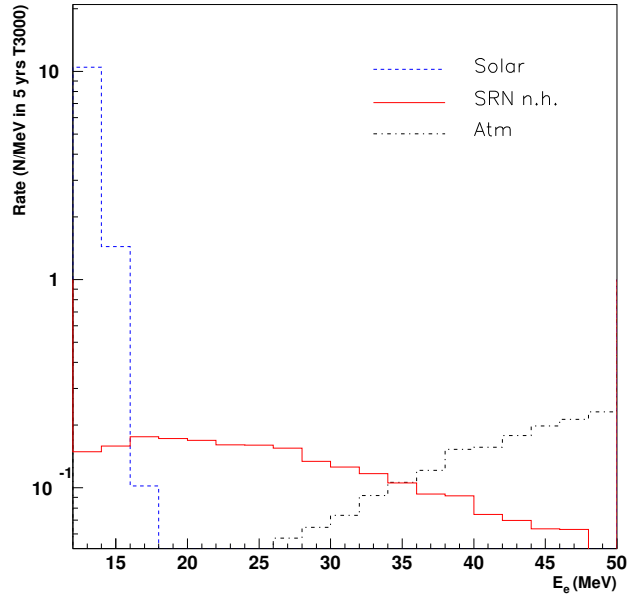


Figure 3. The simulated electron (positron) event spectrum due to solar neutrinos (blue dashed), atmospheric flux (black dot-dashed) and SRN neutrinos (red solid), versus the electron (positron) energy. A normal neutrino mass hierarchy (n.h.) and large  $\theta_{13}$  is assumed. Results are for ICARUS T3000.

In Figure 5 we give the different contributions to the energy spectrum due to  $\nu_e$  and  $\bar{\nu}_e$  charged current interactions and elastic scattering, summed over all neutrino/antineutrino species. As we already mentioned the SRN signal at an ICARUS-like detectors is almost entirely due to  $\nu_e$  charged current interactions.

A change of the values of  $\theta_{13}$  or  $\theta_{12}$  affects the expected signal quite differently. Since the solar neutrino background is too high for neutrino energies lower than 16 MeV, for a typical SN II spectrum and even in the best case of a maximal  $\nu_x \rightarrow \nu_e$  oscillation the contribution of all SN II at redshift larger than 1.5 cannot be detected. In fact, for a  $\nu_x$  effective temperature at the neutrinosphere of 8 MeV, we estimate that for  $z = 1$  a 15% fraction of the total  $\nu_x$  flux produces electron charged current events with energy above the 16 MeV threshold, while this fraction is only 1% for  $z = 2$  sources. This implies that the expected signal is very weakly depending on the star formation rate at redshift larger than 1. This feature is clearly seen in Figure 6 where we show how the SRN spectrum versus the electron (positron) energy changes when varying the star formation slope parameters. The dependence on  $\alpha$  is more pronounced. The total

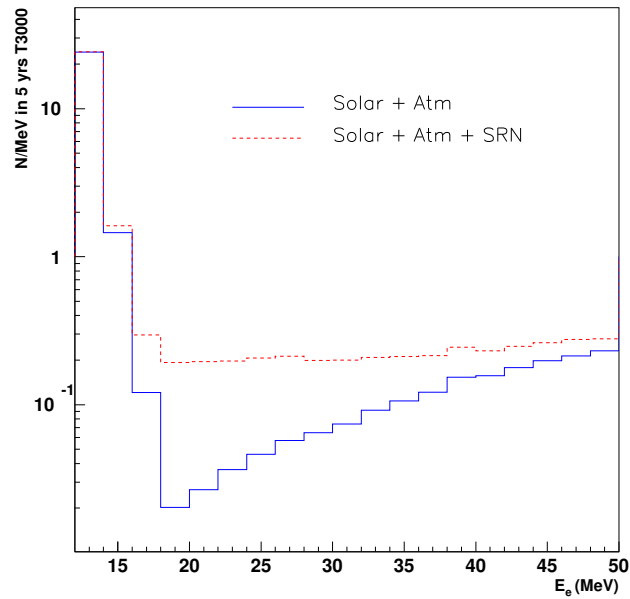


Figure 4. The total event spectrum compared to background due to solar plus atmospheric neutrinos for ICARUS T3000 with a normal neutrino mass hierarchy and large  $\theta_{13}$ .

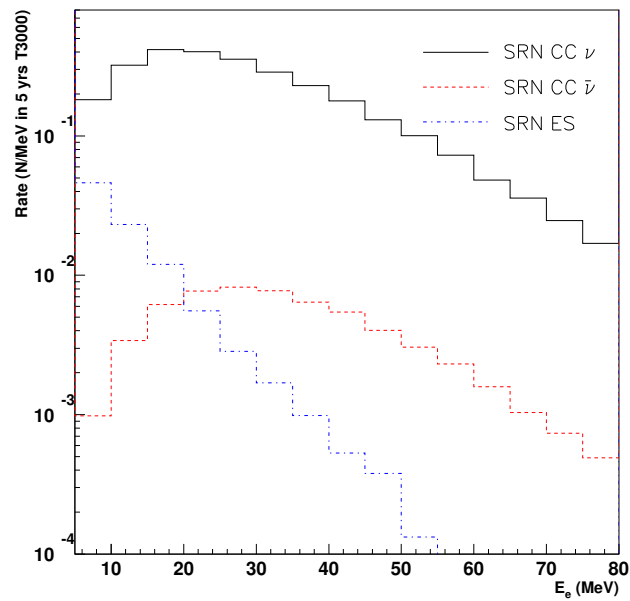


Figure 5. The relative contribution of  $\nu_e$  charged current (black solid line),  $\bar{\nu}_e$  charged current (red dashed) and elastic scattering summed over all neutrino species (blue dot-dashed) for each electron (positron) energy bin (ICARUS T3000).

number of SRN events changes by a factor 20% with respect to the result for  $\beta = 2.5$ , when  $\beta$  varies in the range 2 - 3.

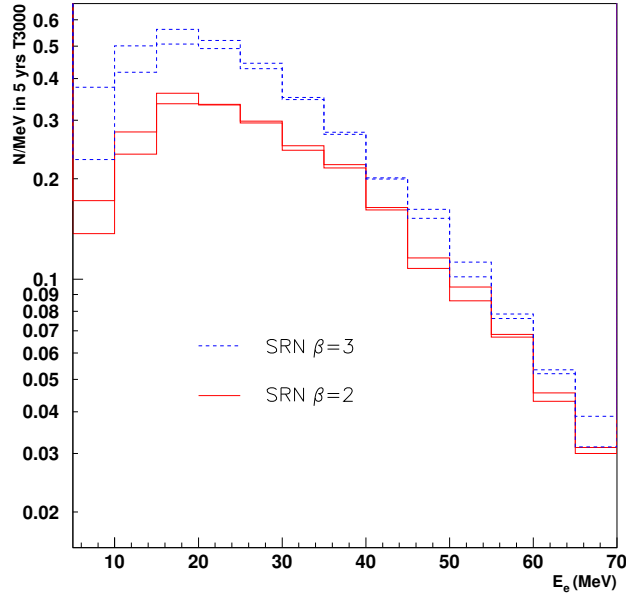


Figure 6. The dependence of the SRN signal on  $\beta$  and  $E_e$  as expected in ICARUS T3000. Upper (blue dashed) curves are for  $\beta = 3$  and, from bottom to top,  $\beta = 0; 2$ . The lower (red solid) curves are for  $\beta = 2$  and the same values of  $\beta$ .

If one integrates the energy spectrum over the selected energy window for a 3 kton liquid Argon detector like ICARUS running for 5 years one obtains  $N_{SRN} = 1.7$  events from SRN flux, to be compared with  $N_{BG} = 0.9$  events from the solar and atmospheric neutrino background. In order to understand the statistical significance of this result we consider the statistical error as given by the Poisson measurement error  $\sigma_{stat}^2 = N_{SRN} + N_{BG}$  and we add in quadrature a systematic error  $\sigma_{sys}$  to account for a 30% uncertainty on the atmospheric flux normalization at low energies and the uncertainty on hep solar neutrino flux as given in [29]. We finally obtain

$$N_{SRN} = 1.7 \pm 1.6; \quad 16 \text{ MeV} < E_e < 40 \text{ MeV} \quad (4.1)$$

This means that ICARUS T3000 may detect the  $\bar{\nu}_e$  signal from past Supernovae at the 1  $\sigma$  level with 5 years of accumulated data.

The above result quite strongly depends on the selected energy window. If we try to push the lower bound towards lower energies the steep rise of the hep and  $^8\text{B}$  neutrino events significantly raises the background. As an example, we find  $N_{SRN} = 1.3$  and  $N_{BG} = 2.4$  for  $14 \text{ MeV} < E_e < 40 \text{ MeV}$ , leading to

$$N_{SRN} = 1.3 \pm 2.1; \quad 14 \text{ MeV} < E_e < 40 \text{ MeV} \quad (4.2)$$

Similarly, a larger upper energy cut gives a less significant result, due to the larger atmospheric neutrino flux. For  $16 \text{ MeV} < E_e < 50 \text{ MeV}$  we find  $N_{\text{SRN}} = 2$  and  $N_{\text{BG}} = 2$ , and correspondingly

$$N_{\text{SRN}} = 2.0 \pm 2.1; \quad 16 \text{ MeV} < E_e < 50 \text{ MeV} \quad ; \quad (4.3)$$

which is slightly better than the result of Equation (4.2), since atmospheric neutrino flux growth with energy is not dramatic.

We note that due to the small number of signal events the total uncertainty is largely dominated by the statistical error, that contributes for 99% of the total error. The remaining 1% is given by the estimated uncertainty on the atmospheric neutrino flux. Therefore, we expect that a sensible improvement of the SRN detection capability of the liquid Argon TPC technique should come from a larger fiducial mass or a longer running time. Recently, ideas about next generation liquid Argon TPC detectors have been put forward [20]. Fiducial masses as large as 50–100 kton may well be envisaged. In this case, for a 100 kton running for 5 years one would get a more than 4 $\sigma$  measurement of the SRN flux

$$N_{\text{SRN}} = 57 \pm 12; \quad 16 \text{ MeV} < E_e < 40 \text{ MeV} \quad ; \quad (4.4)$$

for a normal neutrino mass hierarchy and a large  $\theta_{13}$  and according to the fiducial model considered in this paper.

As a final remark we consider the effect of the different neutrino oscillation schemes summarized in Table 1. In Figure 7 we show the expected SRN event spectrum for normal mass hierarchy and large  $\theta_{13}$  and for inverted mass hierarchy and/or small  $\theta_{13}$ . In particular the expected event rate in the energy range  $16 < 40 \text{ MeV}$  for cases II and III is now  $N_{\text{SRN}} = 1.3 \pm 1.5$ . As expected, this value is smaller than for scenario I, since the electron neutrino flux is shifted toward lower energies, leading to a less than 1 detection for a 3 kton detectors in 5 years. This result shows that it is not possible to distinguish among the three oscillation patterns considered so far, at least with the considered Argon mass and data taking time. Differently, for a 100 kton detector and a running of 5 years we get for Scenario II of Table 1

$$N_{\text{SRN}} = 43 \pm 12; \quad 16 \text{ MeV} < E_e < 40 \text{ MeV} \quad ; \quad (4.5)$$

Comparing this result with Equation (4.4) we see that provided the star formation rate is independently fixed by other observations the different neutrino mass hierarchy may be distinguished by SRN observation at the level of 1 $\sigma$  only.

## 5. Conclusions

In this paper we have studied the possibility of detecting the SRN flux signal at experiments like ICARUS, based on a liquid Argon TPC technique. In the relevant energy range, the leading interaction is the charged current  $\nu_e$  scattering on Argon nuclei, which is revealed via the observation of the produced electron with full detection efficiency for electron energies higher than 5 MeV. Differently than experiments such as

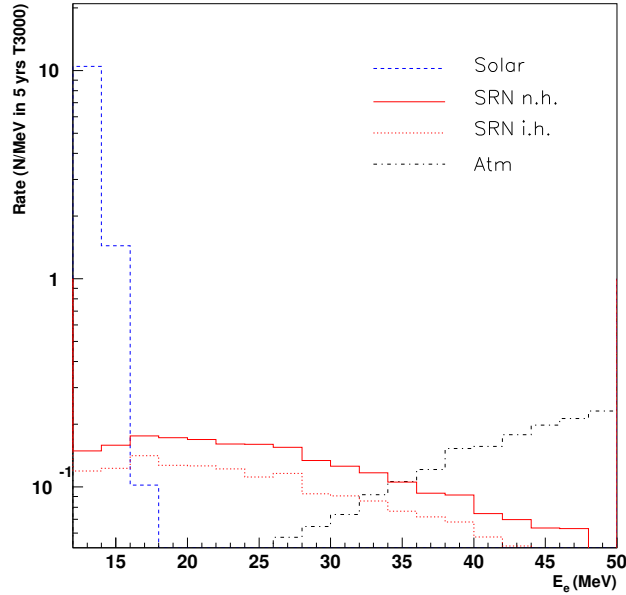


Figure 7. The electron (positron) spectrum for a neutrino normal mass hierarchy and large  $\theta_{13}$  mixing angle (upper red solid curve) and for inverted mass hierarchy (i.h., lower red dotted curve) and/or small  $\theta_{13}$ . The simulation is for ICARUS T3000.

Super-Kamiokande or KamLAND, the SRN flux would be therefore constrained in the  $\nu_e$  component by this experimental technique.

The main detection problem is represented by competing backgrounds. Indeed, below 16 MeV the solar neutrino flux, in its  $^8\text{B}$  and hep components, is larger than the expected SRN signal by orders of magnitude. Similarly, at high energies ( $> 40$  MeV) the atmospheric neutrino flux is largely dominating the total neutrino flux. Nevertheless, we have seen that mainly depending on the star formation rate at  $z \sim 1$  and more weakly on the neutrino oscillation pattern inside the SN II, there can be an electron energy window from 16 MeV to 40 MeV where the SRN neutrino flux is larger than backgrounds. Using a reference model for SRN flux which is presently compatible with the experimental bound on  $\nu_e$  flux from relic SN II obtained by Super-Kamiokande, and which is also well motivated by astronomical observation, the SRN flux may be observed by a 3 kton detector like ICARUS at the 1 level with five years of data taking. Because of the very few events expected in this case, the main source of uncertainty is due to the statistical error. A larger statistical significance will be obtained by next generation, large mass liquid Argon TPC detectors, which can be at the level of 4 for a 100 kton experiment.

## Acknowledgments

We kindly acknowledge G. Battistoni, A. Ferrari, T. Montanuli and P. R. Sala, for providing us the low energy atmospheric neutrino flux, simulated with FLUKA Monte Carlo package. We also thank L. Coraggio for useful discussions on Argon excited nuclear state spectrum.

## References

- [1] Hirata K et al 1987 Phys. Rev. Lett. 58 1490
- [2] Bionta R M et al 1987 Phys. Rev. Lett. 58 1494
- [3] Janka H T et al 2002 Explosion mechanisms of massive stars: a critical review of possibilities and perspectives Preprint astro-ph/0212314
- [4] Super-Kamiokande Collaboration web page: <http://www-sk.icrr.u-tokyo.ac.jp/doc/sk/index.html>
- [5] SNO Collaboration web page: <http://www.sno.phy.queensu.ca/>
- [6] KamLAND Collaboration web page: <http://www.awa.tohoku.ac.jp/html/KamLAND/>
- [7] Aglietta M et al 2002 Nucl. Phys. Proc. Suppl. B 110 410
- [8] Aprili P et al 2002 The Icarus Experiment: a second generation proton decay experiment and neutrino observatory at the Gran Sasso Laboratory Preprint CERN-SPSC-2002-027, CERN-SPSC-P-323. Web page: <http://www.aquila.infn.it/icarus/>
- [9] Gilbotella I and Rubbia A 2004 Decoupling Supernova and neutrino oscillation physics with LAr TPC detectors Preprint hep-ph/0404151
- [10] Totani T, Sato K and Yoshii Y 1996 Astrophys. J. 460 303
- [11] Malaney R A 1997 Astrophys. J. 460 125
- [12] Hartmann D H and Woosley S E 1997 Astrophys. J. 460 137
- [13] Kaplinghat M, Steigman G and Walker T P 2000 Phys. Rev. D 62 043001
- [14] Ando S, Kato K and Totani T 2003 Astrophys. J. 587 307
- [15] Malek M et al 2003 Phys. Rev. Lett. 90 061101
- [16] Strigari L et al 2004 JCAP 0403 007
- [17] Baldry I K and Glazebrook K 2003 Astron. J. 126 1483
- [18] Glazebrook K et al 2003 Astrophys. J. 587 55
- [19] Rubbia C 1977 The Liquid Argon time projection chamber: a new concept for Neutrino Detectors Preprint CERN/77-08
- [20] Rubbia A 2003 Experiments for CP-violation: A giant liquid Argon scintillation, Cerenkov and charge imaging experiment?, Proc. II International Workshop on Neutrino Oscillations in Venice, (Venice) 321;  
Ereditato A and Rubbia A 2004 Ideas for future liquid Argon detectors, to appear in Proc. Third International Workshop on Neutrino-Nucleus Interactions in the Few GeV Region, NUINT04 (Gran Sasso);  
Ereditato A and Rubbia A 2004 Ideas for a next generation liquid Argon TPC detector for neutrino physics and nucleon decay searches, Memorandum to the Special SPSC Session in Villars
- [21] Freedman W L et al 2001 Astrophys. J. 553 47
- [22] Spergel D N et al 2003 Astrophys. J. Suppl. 148 195
- [23] Lunardini C and Smirnov A. Yu. 2003 JCAP 0306 009
- [24] Fogli, G L et al 2004 Phys. Rev. D 69 017301
- [25] Om and W E, Pizzochero P M, Bortignon P F and Broglia R A 1995 Phys. Lett. B 345 343
- [26] Kolbe E, Langanke K, Martinez-Pinedo G and Vogel P 2003 J. Phys. G 29 2569
- [27] ENSDF Database 2004 web page: <http://www-origina.lnndc.bnl.gov/nndc/ensdf/>
- [28] Amoruso S et al 2004 Eur. Phys. J. C 33 233

- [29] Bahcall J N and Pinsonneault M H 2004 Phys. Rev. Lett. 92 121301
- [30] Bahcall J N web page: <http://www.sns.ias.edu/~jnb/>
- [31] Bahcall J N et al 1996 Phys. Rev. C 54 411
- [32] Battistoni G private communication
- [33] Fasso A, Ferrari A, and Sala P R 2000 Proc. Monte Carlo 2000 Conference (Lisbon) (Kling A, Barao F, Nakagawa M, Tavora L and Vaz P editors Springer-Verlag Berlin) 159;  
Fasso A, Ferrari A, Ranft J, and Sala P R 2000 *ibidem* 955